Influence of Hydrogen Bond Formation on the Photophysics of *N*-(2,6-Dimethylphenyl)-2,3-naphthalimide

Attila Demeter,* László Ravasz, and Tibor Bérces

Institute of Chemistry, Chemical Research Center, Hungarian Academy of Sciences, 1025 Budapest, Pusztaszeri u. 59-67 Hungary

Received: January 21, 2004; In Final Form: March 12, 2004

The photophysics of *N*-(2,6-dimethylphenyl)-2,3-naphthalimide (DMPN) has been investigated in the presence of methanol or fluorinated aliphatic alcohols in *n*-hexane and carbon tetrachloride solvents. Consecutive two-step hydrogen bonded complex formation is observed in the presence of alcohols. Equilibrium constants are determined for the formation of singly and doubly complexed species. The UV absorption and fluorescence spectra for the singly and doubly complexed DMPN are derived from the measured absorption and fluorescence spectra, respectively, by means of the equilibrium constants. It is concluded from the results that the spectroscopic properties (singlet excitation energy and Stokes shift) of the complexed species are significantly influenced by the Gibbs energy change in the complexation reaction. Quantitatively, a linear relationship is found between the difference of singlet excitation energy of the complexed and uncomplexed species on one hand and the Gibbs energy change in the complexation reaction on the other hand. This observation is explained by means of an energy cycle and Abraham's hydrogen-bond acidity/basicity model. Hydrogen-bond basicity values are determined for singlet excited DMPN and its singly complexed derivative with hexafluoro-2-propanol. Such hydrogen-bond basicity values of excited states are useful for predicting equilibrium constants for complex formation of the given excited state with other hydrogen bond donors. The photophysical properties of DMPN are strongly influenced by hydrogen bond formation. The fluorescence yield increases dramatically with complex formation, which is caused by an increase in the activation energy of the temperature enhanced intersystem crossing and internal conversion processes.

Introduction

The photophysics of 1,2-, 2,3-, and 1,8-naphthalimides and their *N*-methyl derivatives were investigated in the past decade in our laboratories.[1−5] All of these compounds emit fluorescence around 400 nm. Under certain conditions, some of the *N*-phenyl derivatives show red-shifted, so-called "long wavelength" (LW) fluorescence beside the "short wavelength" (SW) emission, and are characterized by short excited state lifetimes which is the result of efficient internal conversion to the ground state. It was suggested that the geometry of the SW state is similar to that of the ground state (i.e., the plane of the aryl group is nearly perpendicular to that of the imide moiety), whereas twisting of the phenyl group toward a coplanar geometry is assumed to be required in the formation of the LW state.

In previous studies of the photophysics of naphthalimides, experimental conditions were varied in a wide range. Experiments were carried out in various solvents and specific solvent effects were observed in alcoholic media. Thus, for instance, larger bathochromic shifts than expected were found in ethanol solvent.[2] This deviation from the Lippert−Mataga relationship may be an indication of hydrogen bond formation in alcoholic solvents, and therefore, the use of alcohols as solvent was avoided in our previous investigations. However, hydrogen bonding is known to play an essential role in chemistry[6] and biology.[7] Formation of intermolecular hydrogen bonding may have a significant influence on the photophysical behavior of various compounds, in particular on that of aromatic heterocyclic[8] and carbonyl compounds.[9,10] Hydrogen bond formation has a different effect on the energies of various excited states; in an extreme case, hydrogen bonding may cause the reversal of close-lying n,π^* and π,π^* states.[11] In addition, the different strength of hydrogen bonding in the ground and excited states may lead to efficient energy dissipation.[9,10,12] In recent studies, the effect on the fluorescence of hydrogen bonding between hydroxyl substituted naphthalimides and nitrogen-heterocyclic compounds was investigated.[13] In addition, hydrogen bonded complexes of aromatic carbonyl compounds[11] and 1,8-dicarboximides[14] were also examined.

In this paper, we study the effect of complexation with alcohols on the spectroscopy and photophysics of a naphthalimide. 2-(2,6-Dimethyl-phenyl)-benzo[*f*]isoindole-1,3-dione (called

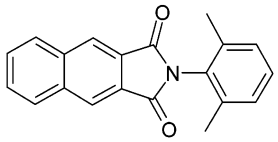

hereafter as *N*-(2,6-dimethylphenyl)-2,3-naphthalimide and designated as DMPN) is selected as the hydrogen bond acceptor. DMPN is a thermally and photochemically stable compound with strong hydrogen bonding ability due to the high electron density on the carbonyl oxygen. DMPN emits only SW luminescence since steric hindrance caused by the bulky methyl substituents prevents rotation toward a coplanar geometry required in the formation of the LW emitting state. Methanol and fluorinated alcohols, in particularly hexafluoro-2-propanol

* To whom correspondence should be addressed. E-mail: demeter@chemres.hu.

10.1021/jp049693m CCC: $27.50
Published on Web 04/21/2004

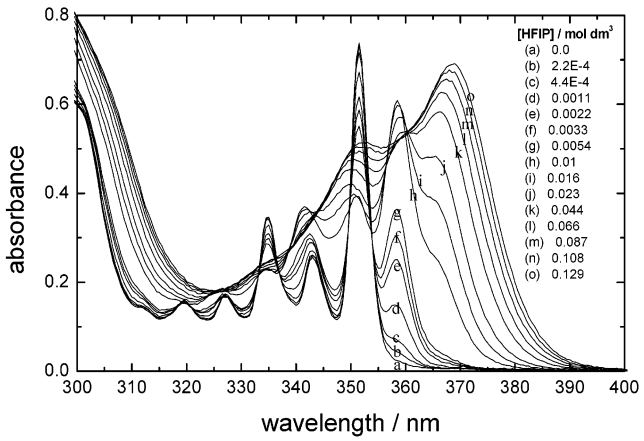

Figure 1. Absorption spectra of DMPN (8×10^{-5} mol dm^{-3}) with various [HFIP] in *n*-hexane.

(i.e., 1,1,1,3,3,3-hexafluoro-2-propanol, HFIP), were used as hydrogen bond donors.

Experimental Section

The preparation and characterization of DMPN was described previously.[3] Carbon tetrachloride for UV−spectroscopy (Fluka) and *n*-hexane for spectroscopy (Merck Uvasol) solvents were used as received. Methanol was obtained from Fluka, and fluorinated alcohols were purchased from Fluorochem Limited and were used without further purification.

Absorption spectra were recorded on a Unicam UV500 spectrophotometer with a resolution typically of 0.2 nm (and exceptionally of 0.5 nm). When necessary, correction was made for dilution caused by the addition of alcohol and for density change due to variation of temperature. The fluorescence spectra were measured with a homemade photon-counting spectrofluorimeter equipped with a Princeton Applied Research 1140 A/B detection system of 1 nm resolution. Room-temperature fluorescence quantum yields were determined relative to that of quinine sulfate ($\Phi_f = 0.546$).[15] Time-resolved fluorescence measurements were made by nanosecond single-photon-counting technique using an Applied Photophysics SP-3 instrument. The short lifetimes were obtained from picosecond time-resolved measurements as reported before.[3] 308 nm (XeCl) light pulses from a Lambda Physik EMG 101 excimer laser were used in all triplet measurements. Transient absorption signals were recorded on an optical line (Xe-lamp − thermostated sample − Applied Photophysics monochromator − RCA 928 photomultiplyer − Hitachi VC6041 digital oscilloscope) mounted perpendicular to the excitation line. Triplet yields were determined using the energy transfer method with perylene as energy acceptor.[16] These measurements were made relative to the triplet yield of *N*-methyl-1,8-naphthalimide ($^3\Phi = 0.95$).[2] Molar absorption coefficients of the triplets were determined relative to that of benzophenone (6600 mol^{-1}dm^{3}cm^{-1}) at 525 nm in acetonitrile.[17]

Results and Discussion

Mechanism and Thermodynamics of Complex Formation. The UV absorption spectrum of DMPN in *n*-hexane was studied with different alcoholic additives in the 0−0.15 mol dm^{-3} concentration range. In Figure 1, the UV absorption spectra of DMPN are given in the presence of hexafluoro-2-propanol of different concentration. The alcohol concentration was kept low; therefore, the solvent polarity could be considered constant and dimerization of the alcohol could be neglected. The UV absorption spectrum of DMPN has a strong vibronic progression with 705 cm^{-1} spacing. The half-width of the vibrational band is relatively narrow (305 cm^{-1} or 3.8 nm). At low [HFIP], increasing alcohol concentration causes a continuous decrease of the 351.4 nm band intensity and simultaneously a new absorption maximum appears at 358.5 nm. An isobestic point is observed around 353.9 nm. Further increase in the HFIP concentration results in the disappearance of the isobestic point, a decrease in the absorption at 358.5 nm, and the appearance of an absorption band at 368.8 nm. These observations can be explained by assuming a two-step consecutive complexation reaction mechanism. The absorption maxima at 351.4, 358.5, and 368.8 nm correspond to the (0−0) transitions of the uncomplexed (N), singly complexed (NX), and doubly complexed (NX_2) species, respectively. (Here X stands for the hydrogen donating alcohol molecule, in the present case HFIP.) The strong red shift observed in the N, NX, NX_2 series indicates the $\pi\pi^*$ character of the uncomplexed and the singly complexed species.

On the basis of spectroscopic results, the complexation mechanism, given in Scheme 1, can be suggested

Scheme 1

$$N + X \overset{K_1}{\longleftrightarrow} NX \tag{1}$$

$$NX + X \overset{K_2}{\longleftrightarrow} NX_2 \tag{2}$$

where K_1 and K_2 are the equilibrium constants for the reversible formation of the singly and doubly complexed species, respectively. Assuming that dimerization of the alcohol is negligible, the expressions for the equilibrium concentrations of species N, NX, and NX_2 are given as

$$[N] = [N]_0 - [NX] - [NX_2] \tag{3}$$

$$[NX] = \frac{K_1[N]_0[X]}{1 + K_1[X] + K_1K_2[X]^2} \tag{4}$$

$$[NX_2] = \frac{K_1K_2[N]_0[X]^2}{1 + K_1[X] + K_1K_2[X]^2} \tag{5}$$

The initial concentration of DMPN, $[N]_0$, can be determined easily from the absorbance of the sample which contains no alcohol. In the case of samples containing alcohol, the absorbance (A) at a given wavelength is described by eq 6

$$A = \epsilon_N[N] + \epsilon_{NX}[NX] + \epsilon_{NX_2}[NX_2] \tag{6}$$

where ϵ_N, ϵ_{NX}, and ϵ_{NX_2} are the molar absorption coefficients of species N, NX, and NX_2, respectively. In an iterative nonlinear fitting procedure, using Marquardt algorithm, K_1, K_2, and the molar absorption coefficients of complexes NX and NX_2 were optimized. In the fitting procedure, the absorbance measured at five selected characteristic wavelengths in samples with various alcohol concentrations was used. A representative fit is presented in Figure 2. The fits are good in general; however, it is to be noted that at high alcohol concentrations (e.g., concentrations higher than 0.15 mol dm^{-3} in case of HFIP in *n*-hexane) calculated curves deviate from the measured points. This may be the result of side reactions, such as the formation and reactions of dimer alcohol. The compartment analysis of the dependence of absorbance on the alcohol concentration at several wavelengths makes the determination of equilibrium

TABLE 1: Room-Temperature Equilibrium Constants (in mol^{-1}dm^3) for the DMPN−HFIP−*n*-Hexane and DMPN−HFIP−Carbon Tetrachloride Systems

solvent:	*n*-hexane		carbon tetrachloride	
K(ground state)	$K_1 = 94 \pm 3$	$K_2 = 13 \pm 3$	$K_1 = 39 \pm 4$	$K_2 = 2.5 \pm 0.5$
K(singlet excited state)	$K_9 = 1500 \pm 130$	$K_{11} = 200 \pm 60$	$K_9 = 340 \pm 60$	$K_{11} = 30 \pm 10$
K(triplet excited state)	$K_{19} = 51 \pm 4$	$K_{20} = 9 \pm 2$		

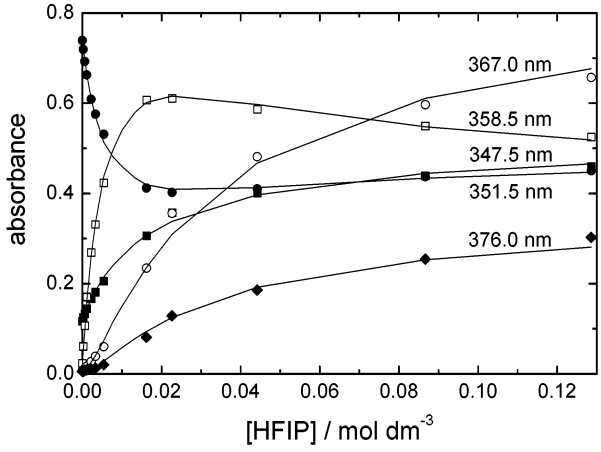

Figure 2. Fitted DMPN (8×10^{-5} mol dm^{-3}) absorbances as a function of HFIP concentration, in *n*-hexane, at five representative wavelengths.

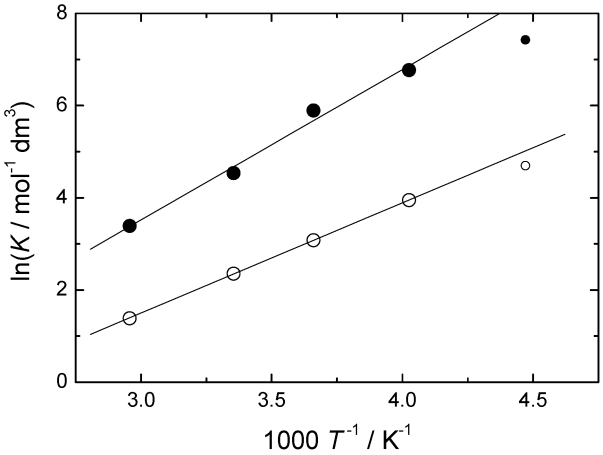

Figure 3. Van't Hoff plots for complexation in the DMPN−HFIP−*n*-hexane system. Full and open circles refer to the first and the second complexation steps, respectively.

TABLE 2: Room-Temperature Photophysical Parameters for the DMPN−HFIP−*n*-Hexane System

species	N	NX	NX_2
^1E/kcal mol^{-1}	81.25	79.3	77.5
$\epsilon(0-0)$/mol^{-1}dm^3 cm^{-1}	6250	7990	8450
Φ_F	0.016 ± 0.002	0.18 ± 0.03	0.45 ± 0.06
Φ_{ISC}	0.42 ± 0.03	0.53 ± 0.04	0.47 ± 0.05
Φ_{IC}	0.56 ± 0.05	0.29 ± 0.07	0.08 ± 0.11
τ/ns	0.46 ± 0.02	1.9 ± 0.2	4.7 ± 0.2
$k_F \times 10^{-8}$/s^{-1}	0.35 ± 0.06	0.95 ± 0.26	1.0 ± 0.2
$k_{ISC} \times 10^{-8}$/s^{-1}	9.1 ± 1.1	2.8 ± 0.5	1.0 ± 0.2
$k_{IC} \times 10^{-8}$/s^{-1}	12.2 ± 1.5	1.5 ± 0.5	0.2 ± 0.3

constants and absorption coefficients more reliable. The optimized room-temperature equilibrium constants and molar absorption coefficients, determined for the DMPN−HFIP−*n*-hexane system, are given in Tables 1 and 2, respectively.

The temperature dependence of the complexation equilibrium constants K_1 and K_2 was studied in the temperature range between −50 and +65 °C. The reaction enthalpy ($\Delta H°$) and reaction entropy ($\Delta S°$) were obtained from the measured temperature dependence of the equilibrium constants in accordance with the van't Hoff equation

$$\ln K = \frac{-\Delta H°}{RT} + \frac{\Delta S°}{R} \qquad (7)$$

The temperature dependence of the equilibrium constants for HFIP complexation in *n*-hexane is presented in Figure 3. From these plots, $\Delta H_1° = -6.5 \pm 0.1$ kcal mol^{-1} and $\Delta H_2° = -4.7 \pm 0.1$ kcal mol^{-1} are obtained. Similar plots, for complexation with perfluoro-*tert*-butyl alcohol (PFTB) in *n*-hexane, yield $\Delta H_1° = -6.8 \pm 0.6$ kcal mol^{-1} and $\Delta H_2° = -5.2 \pm 0.5$ kcal mol^{-1}. It can be seen from Figure 3 that the K values at the lowest temperature are lower than expected from the rest of the data; these data were not taken into account in determining the thermodynamic parameters. Similar deviations were also observed at the lowest temperature in the PFTB complexation system where only approximate values could be derived. The deviation indicates a change in the mechanism with temperature, such as for instance a change in the kinetics of the complex formation step from activation controlled rate at higher temperature to a diffusion controlled rate at low temperature.[10]

As expected, the second complexation step is less exothermic than the first one. Our $\Delta H_1°$ values determined in *n*-hexane can be compared with $\Delta H° = -5.9$ kcal mol^{-1} obtained by Kivinen et al.[18] for the acetone − HFIP system in carbon tetrachloride and $\Delta H° = -8.0 \pm 0.8$ kcal mol^{-1} reported by Sherry and Purcell[19] for the acetone − PFTB system in *n*-hexane.

The reaction entropies of $\Delta S_1° = -12.4 \pm 1.8$ cal mol^{-1} K^{-1} and $\Delta S_2° = -11.3 \pm 1.0$ cal mol^{-1} K^{-1} were determined for the complexation processes in the DMPH−HFIP−*n*-hexane system. Similar values were obtained by us for the DMPH−PFTB−*n*-hexane system ($\Delta S_1° = -12.3 \pm 2.1$ cal mol^{-1} K^{-1} and $\Delta S_2° = -11.3 \pm 2.1$ cal mol^{-1} K^{-1}) and were reported in the literature[18,20] for the other hydrogen-bond formation processes where three translational and three rotational degrees of freedom are lost in the reaction.

Absorption and Fluorescence Spectra of Complexed Species. The knowledge of K_1 and K_2 equilibrium constants of complex formation allows us to derive the spectra for the singly complexed and doubly complexed species. Using the DMPN absorption spectrum, as well as the DMPN spectra measured in the presence of small alcohol concentration (where the singly complexed species dominates) and relatively high alcohol concentration (where the doubly complexed compound prevails), the spectra of the complexed NX and NX_2 species are obtained by an iterative procedure. The fluorescence spectra of the complexed species were obtained by a similar iterative procedure from the fluorescence spectra of DMPN and DMPN spectra measured in the presence of small and relatively high alcohol concentrations.

The absorption spectra of DMPN and of the complexed species in the DMPN−HFIP−*n*-hexane system are presented in Figure 4. It is clear from the figure that the characteristics of the spectra of the complexed species are very similar to those of the DMPN. All three spectra are structured with similar progression and relative intensities of vibronic bands. Slight broadening of the bands can be seen in the series of N, NX, and NX_2. The molar absorption coefficients increase by about

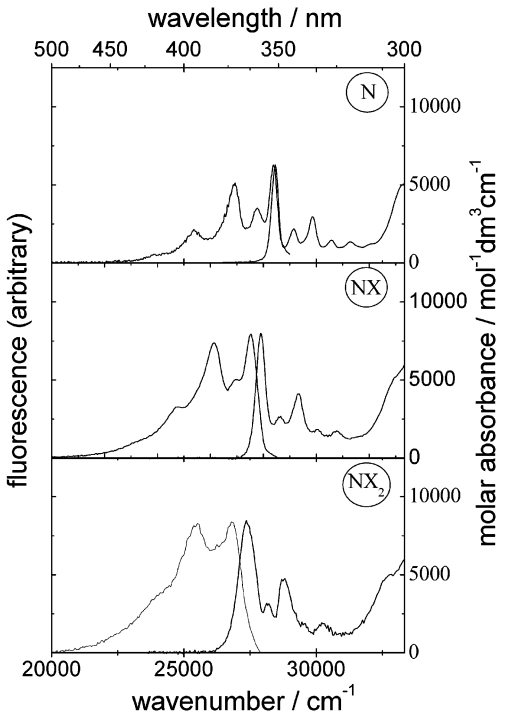

Figure 4. Absorption and fluorescence spectra of DMPN and the complexed species in the DMPN−HFIP−*n*-hexane system.

35% from N to NX_2. The (0−0) absorption band is shifted considerably as a result of complex formation: the shift is 7.1 and 6.9 nm in the first and second complexation step, respectively. (For comparison, the solvatochromic shift of the (0−0) absorption band of DMPN is 7.1 nm when changing the solvent from *n*-hexane to acetonitrile.)

The fluorescence spectra of DMPN and of the complexed species formed in the DMPN−HFIP−*n*-hexane system are also shown in Figure 4. The fluorescence spectrum of DMPN is mirror symmetric to the absorption one, with a very small Stokes shift (less than one nm), indicating that the relaxation in the excited state is almost negligible. The mirror symmetry is also observed for the complexed species; however, the Stokes shift is somewhat bigger, the structure is less pronounced, and the vibronic bands are broader than those of DMPN. The fluorescence quantum yields increase considerably with the complexation (see Table 2).

The complexation of DMPN was studied also with a number of alcohols other than HFIP. These alcohols included PFTB, 1H,1H,7H-dodecafluoroheptan-1-ol (DFH), 2,2,3,3,3-pentafluoropropan-1-ol (PFP), 2,2,2-trifluoroethanol (TFE), and methanol (MET). Equilibrium constants of complex formation and spectroscopic properties of complexed species were determined and the main results are given in Table 3. In the table, the solvents are listed in the order of increasing hydrogen bond donating ability. (See the hydrogen-bond acidity values in the second column.) In this sequence, the equilibrium constants for the first as well as for the second complexation steps increase which indicates a decrease in the Gibbs energy change (i.e., progressively more negative ΔG_1° and ΔG_2° values) of complexation in the series. In the case of the first complexation step, there is significant red shift observed in the location of the absorption and fluorescence maxima. A moderate increase in the Stokes shift is also found. It appears from these observations that the spectroscopic properties of the complexed species are significantly influenced by the Gibbs energy change in the reaction. Probably similar conclusions are valid for the second complexation step too. (The Stokes shift observed for NX_2 is around 350 cm^{-1}; however, the accuracy in the determination is not good enough to draw conclusion regarding its tendency.)

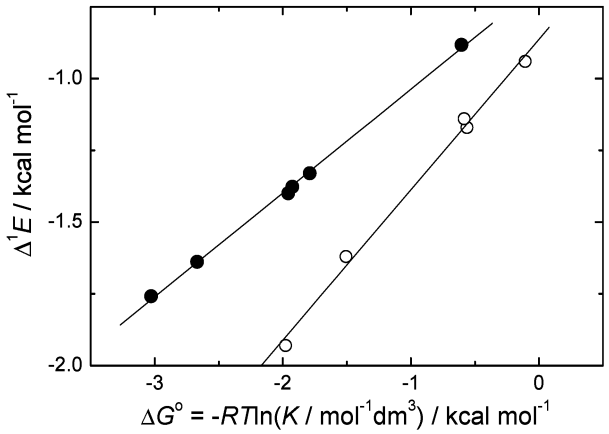

Figure 5. Singlet excitation energy difference of complexed and uncomplexed species (Δ^1E) as a function of Gibbs energy change in complex formation in the DMPN−alcohol−*n*-hexane system at room temperature. Meaning of the symbols is the same as in Figure 3. The sequence of alcohols from right to left is MET, TFE, PFP, DFH, HFIP, and PFTB.

Hydrogen-Bond Basicity of the Ground and Singlet Excited State of N and NX. In Figure 5, the singlet excitation energy difference of the complexed and uncomplexed species (Δ^1E) is plotted as a function of the Gibbs energy change in complex formation ($\Delta G^\circ = -RT \ln K$) at room temperature in *n*-hexane. The data indicate that linear correlation exists between these two quantities. Similarly good linearity is obtained in carbon tetrachloride. To explain this linearity, the energy diagram for complex formation in the ground state and in the excited state (Figure 6) has to be considered, in a manner similar to that presented for heterolytic dissociation processes by Förster[21,22] (The following consideration refers to the first complexation step; however, analogous equations hold also for the second step.)

TABLE 3: Room-Temperature Equilibrium Constants and Spectral Parameters for the DMPN−Alcohol−*n*-Hexane Systems with Different Alcohols

		N↔NX			NX↔NX_2		
alcohol	α^H_2	K_1/ $mol^{-1}dm^3$	(0−0) absorpt. max./ cm^{-1}	Stokes shift/ cm^{-1}	K_2/ $mol^{-1}dm^3$	(0−0) absorpt. max./ cm^{-1}	Stokes shift/ cm^{-1}
none			28459	85			
MET	0.43[a]	2.8	28163	110	1.2	27860	350
TFE	0.57[a]	21	28016	129	2.7	27780	400
PFP	0.64[b]	26.5	28003	136	2.6	27600	400
HFIP	0.77[a]	94	27995	137	13	27910	320
PFTB	0.88[c]	173	27912	145	29	27270	300

[a] Reference 23b. [b] This work. [c] Estimated from results of ref 19.

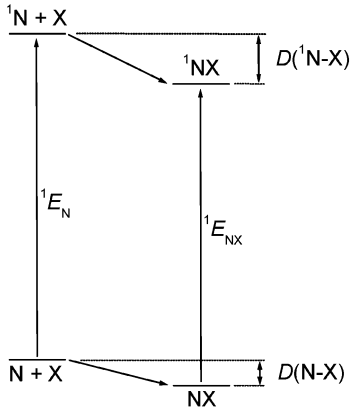

Figure 6. Energy cycle involving ground-state NX and singlet excited state ^{1}NX hydrogen bonded complexes as well as their dissociation products. ^1E_N and $^1E_{NX}$ are the singlet excitation energies of N and NX, respectively, whereas D(N−X) and $D(^1$N−X) are the corresponding bond dissociation energies.

The basic thermodynamic equation for the Gibbs energy change in the formation of ground-state NX from the components maybe given as

$$-RT \ln K_1 = \Delta G_1^\circ = \Delta H_1^\circ - T\Delta S_1^\circ \tag{8}$$

Similarly, for the formation of singlet excited ^{1}NX from excited ^{1}N and X

$$^1\mathrm{N} + \mathrm{X} \overset{K_9}{\longleftrightarrow} {}^1\mathrm{NX} \tag{9}$$

the Gibbs energy change is

$$-RT \ln K_9 = \Delta G_9^\circ = \Delta H_9^\circ - T\Delta S_9^\circ \tag{10}$$

An analogous relationship holds also for the formation of doubly complexed singlet species

$$^1\mathrm{NX} + \mathrm{X} \overset{K_{11}}{\longleftrightarrow} {}^1\mathrm{NX}_2 \tag{11}$$

From eq 8 and 10 one obtains

$$-RT\,(\ln K_9 - \ln K_1) = \Delta G_9^\circ - \Delta G_1^\circ = \Delta H_9^\circ - \Delta H_1^\circ - T(\Delta S_9^\circ - \Delta S_1^\circ) \tag{12}$$

Abraham[23] has expressed log K of a complexation process, in carbon tetrachloride at 298 K, as a function of the product of the solute hydrogen-bond acidity (α_2^H) and the hydrogen-bond basicity (β_2^H)

$$\log K = 7.354\alpha_2^H\beta_2^H - 1.094 \tag{13}$$

Using this type of relationship, ln K_1 and ln K_9 may be given, in a generalized form

$$\ln K_1 = C_2\alpha_2^H\beta_2^H(\mathrm{N}) - C_1 \tag{14}$$

and

$$\ln K_9 = C_2\alpha_2^H\beta_2^H(^1\mathrm{N}) - C_1 \tag{15}$$

where $C_2 = 2.303 \times 7.354 = 16.933$ and $C_1 = 2.303 \times 1.094 = 2.519$ for carbon tetrachloride solvent at 298 K temperature. Substituting α_2^H from eq 14 into eq 15, an expression is obtained for ln K_9 which may be used in rewriting eq 12

$$\Delta H_9^\circ - \Delta H_1^\circ = RT\frac{\beta_2^H(N) - \beta_2^H(^1\mathrm{N})}{\beta_2^H(\mathrm{N})}(\ln K_1 + C_1) + T(\Delta S_9^\circ - \Delta S_1^\circ) \tag{16}$$

Considering the energy cycle involving the ground states and excited states of N and NX (see Figure 6), it can be shown that $\Delta H_9^\circ - \Delta H_1^\circ$ {which equals D(N−X) $-D(^1$N−X)} may be replaced by the difference of the singlet excitation energies of NX and N, i.e., $\Delta^1E = {}^1E_{NX} - {}^1E_N$. Moreover, the entropy change in complexation is expected to be similar for the singlet excited and ground-state species; therefore, $(\Delta S_9^\circ - \Delta S_1^\circ)$ is negligible and $T(\Delta S_9^\circ - \Delta S_1^\circ)$ may be omitted on the right-hand side of the equation. Thus, eq 16 can be replaced by eq 17a

$$^1E_{NX} - {}^1E_N = \frac{\beta_2^H(^1\mathrm{N}) - \beta_2^H(\mathrm{N})}{\beta_2^H(\mathrm{N})}\Delta G_1^\circ - RT\frac{\beta_2^H(^1\mathrm{N}) - \beta_2^H(\mathrm{N})}{\beta_2^H(\mathrm{N})}C_1 \tag{17a}$$

The analogous equation for the second complexation step is

$$^1E_{NX_2} - {}^1E_{NX} = \frac{\beta_2^H(^1\mathrm{NX}) - \beta_2^H(\mathrm{NX})}{\beta_2^H(\mathrm{NX})}\Delta G_2^\circ - RT\frac{\beta_2^H(^1\mathrm{NX}) - \beta_2^H(\mathrm{NX})}{\beta_2^H(\mathrm{NX})}C_1 \tag{17b}$$

These equations demonstrate that, at constant temperature, linear correlation is expected between the singlet excitation energy difference of the complexed and uncomplexed species on one hand and the Gibbs energy change in the complexation process (or alternatively the logarithm of the equilibrium constant for complex formation) on the other hand. This agrees with what has been found experimentally (see Figure 5).

Equation 12 and the analogues equation for the formation of the doubly complexed species offer some further application. Namely, a treatment based on an energy cycle, analogous to the well-known Förster cycle,[21,22] can be used to derive K_9 and K_{11}, the equilibrium constants for the formation of singlet excited singly and doubly complexed species. Neglecting $T(\Delta S_9^\circ - \Delta S_1^\circ)$, replacing $(\Delta H_9^\circ - \Delta H_1^\circ)$ by $({}^1E_{NX} - {}^1E_N)$, as discussed above, and using the known values of the ground-state equilibrium constant and the singlet excitation energy difference $({}^1E_{NX} - {}^1E_N)$, one can calculate the equilibrium constant for the singlet excited species. Such calculated K values are given in Table 1.

Equation 13 or the generalized eq 14 offers a simple technique to characterize complexation equilibria provided that the hydrogen-bond solute parameters are known for the hydrogen donor and hydrogen acceptor species. Following earlier studies,[19,24] Abraham[23] and co-workers established the α_2^H (hydrogen-bond acidity) and β_2^H (hydrogen-bond basicity) scales which became widely accepted. In addition, considerable theoretical efforts were made to predict these hydrogen-bond solute parameters.[25] Moreover, it was shown[26] that the α_2^H is in excellent correlation with the maximum of the electrostatic potential on the surface of the corresponding molecule.

Originally the α_2^H and β_2^H solute scales had been set up using log K values for complexation measured in carbon tetrachloride (see eq 13). No hydrogen-bond basicity parameter has been reported so far for DMPN. To obtain β_2^H values for DMPN and its complexed species, equilibrium constants for complex

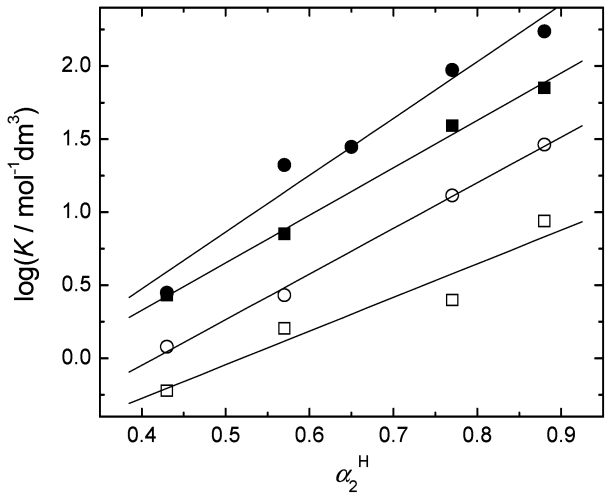

Figure 7. Plot of the logarithm of the equilibrium constant for complexation as a function of hydrogen-bond acidity, in accordance with eq 14 and 15. Circles and squares indicate results obtained in *n*-hexane and carbon tetrachloride, respectively. Full and open symbols refer to the first and second complexation steps, respectively. The sequence of alcohols from left to right is MET, TFE, DFH, HFIP, and PFTB.

formation with methanol and fluorinated alcohols (listed previously) were determined in CCl_4. Determinations of the *K* values were made in the same way as described for the experiments in *n*-hexane. The hydrogen-bond basicity values of N and NX were calculated from eq 13 using the K_1 and K_2 equilibrium constants, respectively, obtained in carbon tetrachloride solvent in this work and the α_2^H values of the alcohols (MET, TFE, DFH, HFIP, and PFTB) taken from the literature.[23b] The α_2^H value of PFTB, for which no data were available, was estimated from literature results[19] to be $\alpha_2^H = 0.88$. The calculated hydrogen-bond basicities showed no dependence on the complexing alcohols and the derived average values were $\beta_2^H(N) = 0.47 \pm 0.02$ and $\beta_2^H(NX) = 0.29 \pm 0.02$. As expected, the hydrogen bonding ability of NX reacting in the second complexation step is lower than that of N participating in the first one (i.e., $\beta_2^H(NX) < \beta_2^H(N)$). However, it is interesting to note that $\beta_2^H(NX)$ does hardly depend on what kind of alcohol is attached to the other hydrogen-bonding site of the naphthalimide structure.

Since eq 13 is based on measurements made in carbon tetrachloride, we used the eq 14 type relationships, with nonfixed C_1 and C_2 coefficients, to interpret the results of equilibrium studies carried out in *n*-hexane. Accordingly, the logarithm of the experimentally determined equilibrium constants for the DMPN−HFIP system is plotted against the appropriate α_2^H values in Figure 7. (The source of the α_2^H values is described above.)

The results of equilibrium studies carried out in carbon tetrachloride are presented for comparison in Figure 7. The intercepts of the straight lines corresponding to the first and second complexation steps are -0.98 ± 0.11 and -1.20 ± 0.06, respectively, in reasonably good agreement with the -1.094 parameter of eq 13 which is based on a large number of equilibrium measurements. From the slopes of the straight lines of the CCl_4 measurements, $\beta_2^H(N) = 0.46$ and $\beta_2^H(NX) = 0.30$ are derived by means of the $C_2 = 7.354$ coefficient taken from eq 13.

For the DMPN−HFIP system in *n*-hexane, similarly good straight lines are obtained both for the first and second complexation steps (see Figure 7); however, discussion of these results requires some assumptions to be made. A reasonable assumption is that the α_2^H and β_2^H scales are independent or are only slightly dependent on the solvent (at least in case of apolar and nonassociative solvents). One obtains, from the intercepts of the log *K* vs α_2^H plots of the data of the first and second complexation steps in *n*-hexane, $C_1 = 1.08 \pm 0.3$ and 1.3 ± 0.2, respectively. These figures agree, within the error limits, with the -1.094 parameter of eq 13 determined in carbon tetrachloride.[23b] Assuming that the $\beta_2^H(N) = 0.47$ value, determined in carbon tetrachloride, can be used to interpret equilibrium results obtained in *n*-hexane, from the slopes of the plots of the straight lines determined in *n*-hexane, a C_2 value of about 14% higher than that determined in carbon tetrachloride is obtained. This result is in quantitative agreement with the 13% difference that is obtained from the comparison of the equilibrium constant measurements made for pyridine *N*-oxide−alcohol complexation in cyclohexane and in carbon tetrachloride.[23c]

TABLE 4: Parameters of Eq 17 and Derived Hydrogen-Bond Basicity Values

solvent	carbon tetrachloride	*n*-hexane
$\beta^H{}_2$ (N)	0.47 ± 0.02	(0.47)[a]
$\beta^H{}_2$ (NX)	0.29 ± 0.02	(0.29)[a]
slope (eq 17a)	0.40 ± 0.16	0.362 ± 0.007
intercept (eq 17a)	-0.9 ± 0.3	-0.67 ± 0.02
$\beta^H{}_2$ (^{1}N)	0.64 ± 0.08	0.64 ± 0.03
slope (eq 17b)	0.55 ± 0.35	0.52 ± 0.02
intercept (eq 17b)	-0.76 ± 0.27	-0.86 ± 0.03
$\beta^H{}_2$ (^{1}NX)	0.46 ± 0.12	0.45 ± 0.03

[a] Assumed to be the same as in carbon tetrachloride.

The knowledge of β_2^H for N and NX allows us to estimate the hydrogen-bond basicities of electronically excited N and NX by means of eqs 17a and 17b, respectively. The plots of the singlet energy difference of the complexed and uncomplexed species against of the Gibbs energy change, in the DMPN−HFIP−*n*-hexane system, yield straight lines (see Figure 5) with slopes and intercepts summarized in Table 4. According to eq 17a and eq 17b, the ratios of $[\beta_2^H(^1N) - \beta_2^H(N)]/\beta_2^H(N)$ and $[\beta_2^H(^1NX) - \beta_2^H(NX)]/\beta_2^H(NX)$, respectively, are directly obtained from the slopes and can be derived, with a known value of C_1, from the intercepts. The ratios originating from the intercepts and the slopes agree within the limits of experimental error; however, in the forthcoming discussion, we use the more accurate slope values. With these ratios, and the above derived ground-state β_2^H values for N and NX (i.e., $\beta_2^H(N) = 0.47$ and $\beta_2^H(NX) = 0.29$), the excited-state hydrogen-bond basicities given in Table 4 are obtained for the DMPN−HFIP system. As far as we know, these values are the first reported hydrogen-bond basicities for excited-state species. For the studied DMPN−HFIP system, the hydrogen-bond basicities of the excited states are equal or close to each other in the two solvents, as expected. Moreover, a higher value is obtained for the excited species compared to the ground-state ones.

Triplet State Properties of Complexed Species. Triplet state properties of complexed species (including triplet yields, equilibrium constants of complex formation and triplet spectra) were studied in detail for the DMPN−HFIP−*n*-hexane system. The triplet yields were measured in *n*-hexane, relative to that of *N*-methyl-1,8-naphthalimide by the energy transfer method using perylene as energy acceptor and 308 nm laser excitation. In a system containing alcohol, the energy transfer method measures the overall triplet yield ($^3\Phi_{overall}$) of various naphthalimide

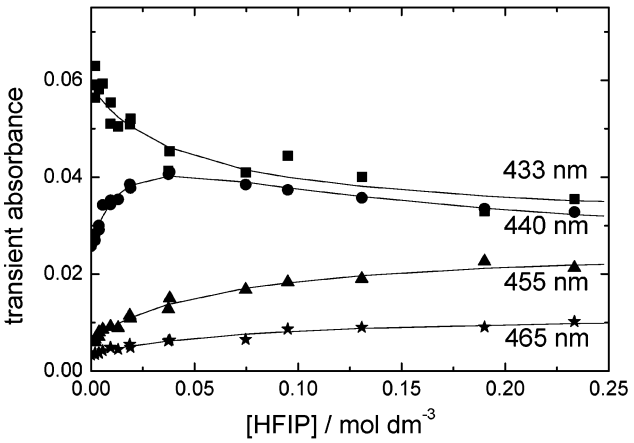

Figure 8. Dependence of transient absorbance on HFIP concentration measured in *n*-hexane at four selected wavelengths.

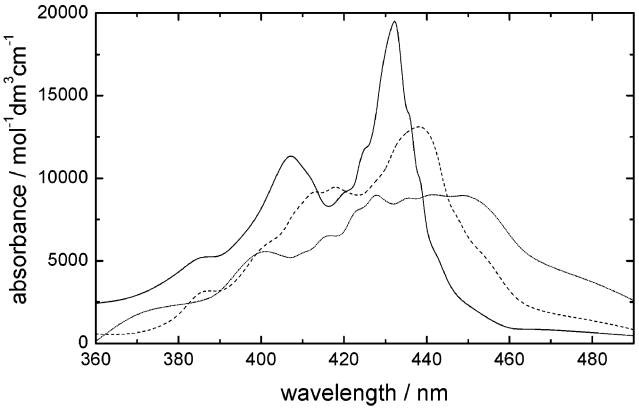

Figure 9. Triplet-triplet absorption spectra of DMPN (full line), singly complexed (broken line) and doubly complexed (dotted line) triplet excited species in *n*-hexane. The hydrogen bond donor is HFIP.

species, i.e., N, NX, and NX_2

$$^3\Phi_{overall} = \rho_N\,^3\Phi_N + \rho_{NX}\,^3\Phi_{NX} + \rho_{NX_2}\,^3\Phi_{NX_2}, \quad (18)$$

where ρ_i stands for the fraction of light absorbed by the *i*th species in the ground state, i.e., $\rho_N = \epsilon_N[N]/\{\epsilon_N[N] + \epsilon_{NX}[NX] + \epsilon_{NX_2}[NX_2]\}$, etc. Triplet yield for the uncomplexed N was measured directly using samples prepared without added alcohol, whereas $^3\Phi_{NX}$ and $^3\Phi_{NX_2}$ were obtained by an iterative procedure from the overall yields measured with samples containing the appropriate alcohol concentrations corresponding to optimum NX and NX_2 concentrations, respectively. The ρ_i parameters were calculated using the known equilibrium constants of complexation as well as the molar absorption coefficients at 308 nm taken from Figure 4. The results of triplet yield determination are given in Table 2.

The determination of the equilibrium constants of complex formation of the triplet excited N and NX with HFIP

$$^3N + X \overset{K_{19}}{\longleftarrow} {}^3NX \quad (19)$$

$$^3NX = X \overset{K_{20}}{\longleftrightarrow} {}^3NX_2 \quad (20)$$

was carried out in an analogous way to that of the ground-state species. The microsecond time scale of the transient absorption measurements is long enough for the development of the equilibrium distribution of the triplet species. On the basis of preliminary experiments, four wavelengths (433, 440, 455, and 465 nm) were selected as characteristic ones for the triplet species ^3N, ^3NX, and $^3NX_2$. Measurements were made with added alcohol varying from 0 up to 0.23 mol dm^{-3} concentration. (The overall absorbance of all samples was set to the same value.) The transient absorbance, extrapolated back to zero time, is corrected for the small difference of the triplet yields of the three species in order to obtain constant overall triplet concentration in the series of the experiments. (The corrections were typically 10−15% and never excided 25%.) The corrected absorbance is plotted as a function of HFIP concentration in Figure 8. An iterative nonlinear fitting procedure, using Marquardt algorithm, is used to obtain K_{19} and K_{20} as well as the molar absorption coefficients of the triplet species. Calculated curves are indicated in the figure. The equilibrium constants of complexation of the triplet species (i.e., K_{19} and K_{20}), obtained from the optimalization procedure, are given in the last row of Table 1. The comparison of the equilibrium constants of the excited- and ground-state species shows that the singlet-state values are much higher, whereas the triplet-state values are lower than the equilibrium constants of the ground-state species. This may be explained by the difference of negative charge density on the oxygen atom of the carbonyl group of the ground state, the excited singlet, and triplet states, respectively. Semiempirical AM-1 computations support this explanation since they show[27] that the negative charge on the oxygen atom is higher for the singlet and lower for the triplet state compared to the ground state.

Triplet−triplet absorption spectrum of DMPN and the overall triplet spectra of samples with added alcohol (at small and relatively high HFIP concentrations, respectively) were measured in *n*-hexane. From the overall spectra and the known K_{19} and K_{20} equilibrium constants, the spectra of the ^3NX and $^3NX_2$ were obtained by an iterative procedure analogous to that used for deriving the ground-state NX and NX_2 spectra. The spectra are shown in Figure 9. Complexation is seen to cause moderate red shift and decrease of the vibronic structure. The oscillator strengths (the integrals of the spectra) are the same for the three species within the uncertainty of measurements. The comparable oscillator strengths indicate that the character of the triplet−triplet transition does not change with complexation.

Photophysics of Excited Complexed Species. Singlet lifetimes were measured for N, NX, and NX_2 in the temperature range of 230−340 K. In these experiments, the excitation wavelength was chosen at the maximum of the corresponding (0−0) absorption band. The room-temperature results are presented in Table 2.

Using the singlet lifetime (τ_F), the fluorescence quantum yield (Φ_F), intersystem crossing quantum yield (Φ_{ISC}), and the internal conversion yield ($\Phi_{IC} = 1 - \Phi_F - \Phi_{ISC}$), the rate coefficients of singlet state depopulating photophysical processes are obtained. The room-temperature rate coefficients are given in Table 2, and the Arrhenius plots of the photophysical processes of the singlet excited species ^1N and $^1NX_2$ are shown in Figure 10. Although the rate coefficients for the reactions of ^1NX show significant uncertainties (due to the fact that samples of NX always contain N and NX_2 "impurities"), however, it is clear from the available data that the characteristic tendencies of the temperature dependence of the rate coefficients of ^1NX are of intermediate nature between those observed for ^1N and $^1NX_2$.

At room temperature, as well as at higher temperature, the excited state lifetime increases considerably with complexation. This increase determines the trend seen in the fluorescence quantum yields, although the fluorescence rate constants show only moderate increase with complexation. At room temperature,

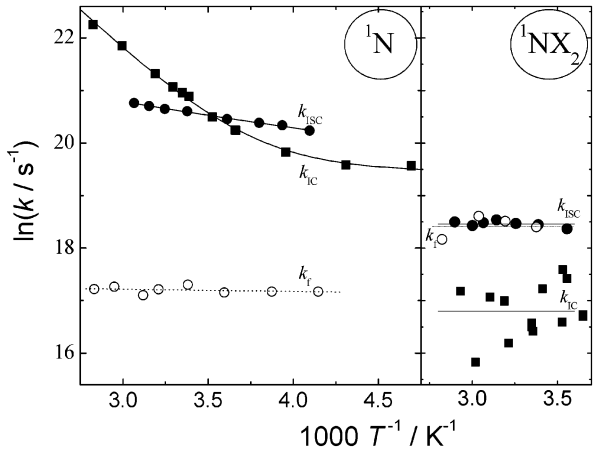

Figure 10. Arrhenius plot of the rate coefficients of photophysical processes for uncomplexed DMPN (^{1}N) and doubly complexed ($^1NX_2$) species in *n*-hexane. The hydrogen bond donor is HFIP.

the increase of the radiative rate coefficients is in accordance with the observed increase of the oscillator strengths of the lowest lying absorption band. As expected, k_F is practically temperature independent.

The temperature dependences of the rate coefficients of uncomplexed ^{1}N and complexed $^1NX_2$ show completely different characteristics. Nonradiative rate coefficients for ^{1}N are temperature dependent, whereas those of $^1NX_2$ are not. Intersystem crossing from ^{1}N to a higher lying triplet state may be responsible for the observed temperature dependence of k_{ISC} (with $A = (4.7 \pm 0.3) \times 10^9$ s^{-1} and $E_a = 0.99 \pm 0.03$ kcal mol^{-1}), in agreement with the observations made in case of *N*-methyl-2,3-naphthalimide.[2] For NX_2, where the singlet excitation energy is lower by 3.1 kcal mol^{-1} (and with a higher nπ^* triplet state energy[3]), temperature enhanced singlet $\rightarrow$ triplet transition is not possible energetically; therefore, only a temperature independent intersystem crossing process occurs.

The temperature dependence of the internal conversion rate coefficient shows complex character: for ^{1}N, a temperature independent process dominates at low temperature ($k_0 = (2.8 \pm 0.2) \times 10^8$ s^{-1}) and a significant temperature enhanced contribution is observed at high temperature (with $A = (2.8 \pm 0.9) \times 10^{13}$ s^{-1} and $E_a = 6.2 \pm 0.2$ kcal mol^{-1}). This fast, temperature enhanced internal conversion process causes the short singlet lifetime of singlet excited DMPN, which is characteristic also for the local excited singlet state of *N*-phenyl-2,3-naphthalimide and its derivatives.[3] The efficient internal conversion of the *N*-aryl-naphthalimides has been explained[3] by the crossing of the S_1 ($^1A_2$) and S_2 ($^1B_1$) excited-state potential energy surfaces. Complexation decreases the energy of the S_1 surface and it influences the S_2 surface as well; as a result, small or no temperature enhanced internal conversion occurs from $^1NX_2$.

Acknowledgment. This work was supported by the Hungarian Science Foundation (OTKA T33102 and T43601).

References and Notes

(1) Valat, P.; Wintgens, V.; Kossanyi, J.; Biczók, L.; Demeter, A.; Bérces T. *J. Am. Chem. Soc*. **1992**, *114*, 946.

(2) Wintgens, V.; Valat, P.; Kossanyi, J.; Demeter, A.; Biczók, L.; Bérces, T. *J. Chem. Soc., Faraday Trans*. **1994**, *90*, 411.

(3) Demeter, A.; Biczók, L.; Bérces, T.; Wintgens, V.; Valat, P.; Kossanyi, J. *J. Phys. Chem*. **1996**, *100*, 2001.

(4) Wintgens, V.; Valat, P.; Kossanyi, J.; Biczók, L.; Demeter, A.; Bérces, T. *J. Photochem. Photobiol. A: Chem.* **1996**, *93*, 109.

(5) Valat, P.; Wintgens, V.; Kossanyi, J.; Biczók, L.; Demeter, A.; Bérces, T. *Helv. Chim. Acta* **2001**, *84*, 2813.

(6) Mellot, C. F.; Davidson, A. M.; Eckert, J.; Cheetham, A. K. *J. Phys. Chem. B* **1998**, *102*, 2530.

(7) Jeffrey, G. A.; Saenger, W. *Hydrogen Bonding in Biological Structures*; Springer: Berlin, 1991.

(8) Herbich, J.; Hung, C.-Y.; Thummel, R. P.; Waluk, J. *J. Am. Chem. Soc*. **1996**, *118*, 3508 and references therein.

(9) Biczók, L.; Bérces, T.; Linschitz, H. *J. Am. Chem. Soc*. **1997**, *119*, 11071.

(10) Yatsuhashi, T.; Inoue, H. *J. Phys. Chem. A* **1997**, *101*, 8166. Yatsuhashi, T.; Nakayima, Y.; Shimada, T.; Tachibana, H.; Inoue, H. *J. Phys. Chem. A* **1998**, *102*, 8657 and references therein.

(11) Burgt, M. J. van der; Jansen, L. M. G.; Huizer, A. H.; Varma, C. A. G. O. *Chem. Phys.* **1995**, *201*, 525.

(12) Sinicropi, A.; Nau, W. M.; Olivucci, M. *Photochem. Photobiol. Sci.* **2002**, *1*, 537; Waluk, J. *Acc. Chem. Res.* **2003**, *36*, 832.

(13) Biczók, L.; Valat, P.; Wintgens, V. *Phys. Chem. Chem. Phys*. **1999**, *1*, 4759. Biczók, L.; Valat, P.; Wintgens, V. *Phys. Chem. Chem. Phys*. **2001**, *3*, 1459.

(14) Sinks, L. E.; Wasielewski, M. R. *J. Phys. Chem. A* **2003**, *107*, 611.

(15) Demas, J. N.; Crossby, G. A. *J. Phys. Chem.* **1971**, *75*, 991.

(16) Demeter, A.; Bérces, T.; Zachariasse, K. A. *J. Phys. Chem. A* **2001**, *105*, 4611 and references therein.

(17) Demeter, A.; Bérces, T. *J. Photochem. Photobiol. A: Chem*. **1989**. *46*, 27.

(18) Kivinen, A.; Murto, J.; Kilpi, L. *Suomen Kemistilehti B* **1967**, *40*, 301.

(19) Sherry, A. D.; Purcell, K. F. *J. Am. Chem. Soc*. **1972**, *94*, 1853; *J. Phys. Chem*. **1970**, *74*, 3535.

(20) Vinogradov, S. N.; Linnell, R. H. *Hydrogen Bonding*; Van Nostrand Reinhold Company: New York, 1971.

(21) Förster, Th. *Z. Electrochemie* **1950**, *54*, 42. Grabowski, Z. R. *J. Luminescence* **1981**, *24/25*, 559.

(22) Schulman, S. G. *Fluorescence and Phosphorescence Spectroscopy: Physicochemical Principles and Practice*; Pergamon Press: Oxford, U.K., 1977.

(23) (a) Abraham, M. H.; Duce, P. P.; Prior, D. V.; Barrat, D. B.; Morris, J. J.; Taylor, P. J. *J. Chem. Soc., Perkin Trans. 2* **1989**, 1355. (b) Abraham, M. H. *Chem. Soc. Rev*. **1993**, *22*, 73. Abboud, J.-L. M.; Sraidi, K., Abraham, M. H.; Taft, R. W. *J. Org. Chem*. **1990**, *55*, 2230.

(24) Drago, R. S.; Wayland, B. B. *J. Am. Chem. Soc*. **1965**, *87*, 3571. Taft, R. W.; Gurka, D.; Joris, L.; Schleyer, P. von R.; Rakshys, J. W. *J. Am. Chem. Soc*. **1969**, *91*, 4801. Drago, R. S.; Vogel, G. C.; Needham, T. E. *J. Am. Chem. Soc*. **1971**, *93*, 6014.

(25) Platts, J. A. *Phys. Chem. Chem. Phys*. **2000**, *2*, 973; *Phys. Chem. Chem. Phys*. **2000**, *2*, 3115.

(26) Hagelin, H.; Murray, J. S.; Brick, T.; Berthelot, M.; Politzer, P. *Can. J. Chem*. **1995**, *73*, 483.

(27) Demeter, A. unpublished AM-1 results.